ERO2.0 modelling of surface roughness effects on molybdenum erosion and re-deposition in PSI-2 linear plasma device

A. Eksaeva[1]*, D. Borodin[1], J. Romazanov[1], A. Kreter[1], A. Pospieszczyk[1], S. Dickheuer[1], S.Möller[1],
B. Göths[1], M. Rasinski[1], U. Knoche[1], A. Terra[1], A. Kirschner[1], I. Borodkina[1], M. Eichler[1], B. Unterberg[1],
S. Brezinsek[1], Ch. Linsmeier[1], E. Vassallo[2], M.Pedroni[2], M. Passoni[2,3], D. Dellasega[2,3], M. Sala[3], F.Romeo[3],
S. Henderson[4], M. O'Mullane[5], H. Summers[5], D. Tskhakaya[6], K. Schmid[7]

[1] Forschungszentrum Jülich GmbH, Institut für Energie- und Klimaforschung – Plasmaphysik, Partner of the Trilateral Euregio Cluster (TEC), Jülich, Germany
[2] Istituto per la Scienza e Tecnologia dei Plasmi, CNR, Milano, Italy
[3] Dipartimento di Energia, Politecnico di Milano, Via Ponzio 34/3, 20133 Milan, Italy
[4] CCFE, Culham Science Centre, Abingdon, OX14 3DB, UK
[5] University of Strathclyde, Dept. of Physics, Glasgow G4 0NG, UK
[6] Czech Academy of Sciences - Institute of Plasma Physics, Prague, Czech Republic
[7] Max-Planck-Institut für Plasmaphysik, D-85748 Garching, Germany

Abstract

Surface morphology of plasma-facing components (PFCs) and its evolution during the plasma irradiation has shown to have a significant effect on the erosion and subsequent transport of sputtered particles in plasma. This in turn can influence the resulting lifetime of PFCs. A model for treatment of the surface roughness effect on the erosion of PFCs has been recently incorporated into the 3D Monte-Carlo ERO2.0 code. First simulations have confirmed significant influence of the assumed surface roughness (both regular and stochastic numerically constructed samples) on both the effective sputtering yields Y_{eff} and the effective angular distributions of sputtered particles. In this study series of experiments at the linear plasma device PSI-2 are conducted to test the surface roughness effect on the sputtering parameters. Graphite samples prepared with 100 nm molybdenum (Mo) layer with various surface roughness characteristic size (R_a = 110 nm, 280 nm, 600 nm and R_a< 20 nm) were exposed to the helium (He) plasma in the PSI-2 linear plasma device at magnetic field of B=0.1T. These PSI-2 experiments were simulated using the ERO2.0 with surface morphology model. Simulations are able to reproduce the experimentally observed significant suppression of erosion for higher R_a values.

1. Introduction

Erosion of plasma-facing components (PFCs) determines their lifetime and affects other plasma-surface interaction (PSI) issues important for ITER [1], like impurity sources, tritium (T) co-deposition with beryllium (Be) or material migration [2]. Surface morphology is shown to have a significant effect on sputtering parameters like effective sputtering yield (Y_{eff}) and angular distributions of the sputtered particles [3, 4], thus erosion is determining the preferential areas of erosion and deposition [5]. The influence of developing surface morphology on the Y_{eff} and transport of sputtered particles was observed in several experiments [6, 7, 8]. Some earlier modelling attempts have reproduced the decrease of the Y_{eff} for a non-smooth surfaces as well as sheath potential distribution modification near the rough surface [9, 10, 11]. The 3D Monte-Carlo code SURO [34] was coupled with PIC simulations of the edge plasma in fusion reactors and has shown a significant influence of the evolving during the irradiation surface morphology on the physical sputtering yield. The recently developed SDTrimSP-3D code was successfully used to simulate the temporal evolution of regular surface structures under ion beam exposure [12], however these approach and the dedicated validation experiment do not include plasma effects like sheath influence on the ion movement close to the rough surface or local transport of the sputtered particles which may lead to an additional re-erosion.

The 3D Monte-Carlo code ERO [13] is an established tool for modelling of the PSI and local impurity transport in the plasma. It considers a wide range of physical processes like physical sputtering of PFCs and transport of sputtered impurities in the plasma (including ionization, recombination, light emission, plasma friction, elastic collisions, etc.). Moreover, it is capable of modelling widely used diagnostics like passive optical spectroscopy or deposition on the quartz-microbalance (QMB) sensor plate, which allows direct simulation of the experimental results. ERO has been applied to toroidal devices like ITER [14] or JET [15], as well as to linear devices like PSI-2 [6], PISCES-B [16], Pilot-PSI [17]. Recently an upgraded version of the code - ERO2.0 [18] - was developed. It uses mostly the same physics as the previous ERO version, however utilizes massive parallelization providing the capability to simulate large number of test particles. ERO2.0 is also capable of processing large and complexly 3D shaped surface geometries, for instance the full ITER and JET-ILW first wall [19, 20]. In our previous work [21] we applied for the first time the same ERO2.0 code to the Mo rough surface on the micro-scale and simulated the surface roughness effect on the erosion on the example of several numerically constructed surfaces. It was shown that sharper (more "filigree") surface structures (both regular and irregular) lead to a significant suppression of the erosion, for instance up to factor 5-6 in the case considered in that work. In the present study experimental validation of this model in experiments in the PSI-2 linear plasma device is in the focus. Developing of a new module for ERO2.0 responsible for the rough surface representation should allow in future combining the modelling on the micrometer-scale and on the machine-scale. The effective sputtering parameters of the rough surface can be derived from micrometer-scale calculations and later be applied as an input for the machine-scale simulations.

Linear plasma devices like PSI-2 [22], PISCES-B [16] or Pilot-PSI [17] are a perfect testbed to investigate PSI processes, due to the simple (in comparison to tokamaks) geometry and continuous operation. All three mentioned devices provide close to the mono-energetic incidence of plasma ions with the incident energy (E_i) controlled by the bias voltage (U_b) applied to the target. The magnetic field $B \approx 0.1T$ is normal to the target. In this study we test the effect of the surface roughness on the erosion by irradiating several molybdenum-deposited (Mo) samples with various surface roughness by the helium (He) plasma in the PSI-2 linear device. Moreover, this experiment is dedicated to validate the developed ERO2.0 surface morphology model. In this work we aim for investigating of the surface roughness effect on the Y_{eff}, angular distribution of sputtered particles, as well as temporal evolution of the surface.

2. ERO2.0 surface morphology model

The rough surface is represented in ERO2.0 by a polygon mesh of surface cells. Each individual cell is assumed flat and smooth (the sputtering yield and the angular distribution of sputtered particles are calculated using the local incidence angle of the plasma flux constant within the cell). The calculated amount of eroded atoms in each cell is distributed between the number of test particles, which are traced later on by ERO during their transport in the local plasma volume until they escape it or hit the wall. Each generated and traced in ERO test particle is a super-particle, consisting of many "real" atoms (particle weight depending on the modelling case). ERO considers the PSI from each surface collision, which includes sputtering (e.g. physical, chemical) of the target material and reflection or deposition of the incident particle. In this study, about 5×10^5 test particles (~2 per cell) were traced on each time step. Particles finally escaped from the surface (e.g. not deposited on the neighboring structures) define the effective sputtering parameters of the rough surface. Various numerical surface topographies can be constructed in ERO2.0: the surface shape can be defined by a formula, or randomly generated as a 3D surface mesh with e.g. certain fractal dimension value D_{fract}. Furthermore, the realistic topographies based on Atomic Force Microscopy (AFM) [23] measurements can also be used. The local surface angle with the magnetic field η (determining the dominant incident plasma ion direction) can vary significantly along the rough surface affecting the angular and energy distributions of sputtered particles on the slopes of fine surface structures on the rough surface. Using η as parameter for sampling of these distributions is natural and was already proved to be useful on the macroscale [33].

It was shown experimentally and in simulations that in the case of oblique ions incidence, sputtered particles tend to keep the direction of the sputtering ions, at least the velocity component parallel to the surface plane [24]. The significance of this effect was discussed in our previous study [21]. It was shown that this effect can reduce the resulting Y_{eff} value by ~20%.

Currently, there are two possibilities for sampling the energy and angular distributions of sputtered particles in ERO2.0. The first – analytical - approach is described in detail in our previous work [21]. In this case both polar $f(\theta)$ and azimuthal $f(\varphi)$ angular distributions are sampled independently according to the analytical formula (e.g. "butterfly" shape for $f(\theta)$ [25]. The energy distribution is sampled according to the Thompson distribution [24] and the sputtering yield value is defined using the Eckstein approximation formulas for the SDTrimSP calculations [26]. Another option implemented recently in ERO2.0 is the direct input from the SDTrimSP code [27]. SDTrimSP calculations provide table data on the sputtering yields with energy and angular distributions of sputtered particles resolved by the incident ion energy E_{in} and angle α. SDTrimSP simulations are conducted for many combinations of materials and these multidimensional data is interpolated during an ERO2.0 run. This method reduces the effort to search for an appropriate analytical approximation of $f(\theta)$ and $f(\varphi)$, providing the information directly. The downside of this approach, however, is the necessity to conduct large amount of SDTrimSP runs before the simulation to prepare a fine enough E_{in}/α mesh. In this work, to maximize precision we use direct input from the SDTrimSP, however, it should be noted that this approach can be too time consuming and data volume demanding to be used in a general case.

3. Validation of the ERO2.0 surface morphology model

In the previous study [21] we have tested the influence of various surfaces by applying ERO to the two following constructed surfaces: 3D cosine peaks and the randomly-generated fractal surfaces with a given fractal dimension D_{fract}. In the first case the Y_{eff} was decreasing with the increase of the aspect ratio of the periodic peaks (height to width ratio). At the same time the angular distribution of the sputtered particles was peaking in the normal to the surface direction. Similar effect was observed for the randomly-generated surface with the growth of the D_{fract}. In both cases the decrease of the Y_{eff} by a factor of ≈ 2-5 was observed in the simulated range of parameters.

The surface evolution under the plasma irradiation is treated in ERO2.0 in the following way. For each surface cell the amount of sputtered/deposited material is calculated. These values are transformed into the sputtered/deposited thickness, with sputtering as a negative contribution and deposition as a positive one. For every vertex a weighted average of sputtered thickness values from all its neighboring faces is calculated and the unity vector of the shift direction is estimated as a weighted average of the neighboring faces normal vectors. After that normal and areas of all surface cell are recalculated based on new vertices positions. A triangular mesh was used for the simulations described. Instabilities like overcrossing of two neighboring faces (example is the border between the top and the side surface of cylinders considered below) are concealed by removing these faces and a corresponding vertex. This reflects the fact that during the sputtering the total amount of material decreases. In order to avoid artifacts connected to sensitivity of sputtering yields to the surface slope an additional smoothing procedure was applied: position of each vertex is calculated as an average of positions of its neighbors (vertices connected to it through a face).

To test the ERO2.0 surface modification algorithm, the results of recently conducted ion beam experiments [12] were utilized. These experiments complement the plasma irradiation experiment discussed below, because they allow excluding other typical for the plasma irradiation processes (surface sheath E-field, angular and energy distributions of incident ions) but the physical sputtering itself. In these experiments silicon (Si) or tantalum (Ta) cylindrical columns (diameter D=100-130 nm, height H = 200 nm) were exposed to an argon (Ar) ion beam of 5 keV energy. Three ion incidence directions were considered: normal to the target surface ($\theta=0°$ $\varphi=0°$), $\theta=45°$ $\varphi=0°$ and $\theta=45°$ $\varphi=15°$ incidence (see Fig.1a). This surface morphology was reproduced in ERO2.0 using a polygon mesh with 500x500 cells, representing an area of 400x400 nm^2 ($\approx$0.64 nm^2 cells, 7-9 atoms in each surface cell). Sputtered particles (5x10^5 test particles, $\approx$3.5x10^5 "real" atoms in each) were traced in a simulation volume of 400x400x210 nm^3 with periodic boundary in both horizontal directions. Particles that have encountered the structures were considered as deposited (100% sticking) with respective effect on the surface evolution. The reflection was considered during the runs, however for energies of the sputtered Si/Ta (<10eV) the reflection coefficients were negligible. The incident beam ions were not traced individually but treated as a homogeneous flux, however with a correction to account for the self-shadowing by the surface structures. Since the surface topography experienced significant evolution, the shadowing pattern was updated each time step (see Fig.1a). For the ERO2.0 validation we have used 1) the case with Ar ions beam normal to the Si cylinder surface (after fluence F=15x10^{20} m^{-2}) and 2) the more complex case of $\theta=45°$ $\varphi=15°$ Ar incidence on Ta structures (after fluence F=7x10^{20}m^{-2}). The comparison of experimental profiles with respective ERO2.0 simulations are shown in Fig.1b. One can see that they are in a good agreement for both Si and Ta cases.

4. PSI-2 experiments on surface roughness: influence on the erosion

PSI-2 is a linear plasma device with a magnetically confined (magnetic field B=0.1T, normal to the target) plasma column of approximately 6 cm diameter. Incident plasma ions energies can be controlled by the bias potential U_b applied to the target. Mass loss measurements of the target provide the information about the net erosion, while the optical spectroscopy measurements near the target surface can help to estimate the gross erosion and give an insight in transport properties such as impurities penetration length or metastable levels population evolution [6]. A quartz microbalance deposition sensor is installed at the distance of 30 cm from the target along the facility axis outside of the plasma column, providing information about the angular distribution of sputtered particles [28]. When interpreted with the ERO modelling, these experiments are capable of giving the understanding of particular PSI and impurity transport processes. In the case at hand, however, the He$\rightarrow$Mo sputtering was too low to produce any significant deposition on the QMB, therefore this diagnostic is not considered.

For the experiments, samples with various predefined roughness Ra values were used. An etching procedure was utilized to produce graphite samples of 1x1cm2 with a rough surface of Ra = 110 nm, 280 nm, 600 nm and a smooth reference of Ra < 20 nm (estimated by AFM) [30]. After the etching a 100 nm layer of Mo was deposited by Pulsed Laser Deposition [35] on the samples. Thanks to the high energy of this deposition technique, a compact layer is grown mimicking the underlying substrate roughness. One can find the Scanning Electron Microscopy (SEM) [31] pictures of the samples before the exposure in the Fig.2a. Two main effects were investigated in the experiments: a) influence of the surface roughness on the Y$_{eff}$; b) influence of the surface roughness on the effective angular distribution of sputtered particles.

The scheme of the experiments is shown in the Fig.3. Irradiating several samples simultaneously was achieved using the tungsten (W) target holder with 8 slots for 1x1 cm^2 samples placed radially symmetric as shown in the Fig.3a. The profiles of the plasma parameters at the PSI-2 have a specific "hollow" shape (minimum of plasma temperature T_e and density n_e at the facility axis, maximum at r $\approx$ 2.5 cm) due to the cylindrical plasma source (Fig.3b). As shown in the Fig.3a, the samples were positioned in the area of maximum flux, all of them experiencing similar exposure conditions. Helium has been chosen as the plasma species for these experiments, as the He$\rightarrow$Mo sputtering yield is comparatively high at low incident energies E_i ($Y_{He\rightarrow Mo} \approx 0.001$ for the $E_i = 90$ eV), while W is not sputtered at all. Moreover, it was important to understand whether the thin Mo layer will be sputtered by the impurities present in the plasma (mainly oxygen). First, to minimize the O content in the plasma we tried to reduce the probability of oxygen (O) desorption during the exposure due to the sample heating by outgassing the samples at 300 °C before the experiment. Furthermore, the typical amount of O in the PSI-2 plasma is about 0.3%, which can lead to an additional erosion of Mo and sputtering of W. In the experiments we used the U_b = -100 V, which after subtracting the plasma potential $U_{plasma} \approx$ -10V was resulting in the He$^+$ impact energy of $E_i \approx$ 90 eV. This is slightly above the sputtering threshold for the O$\rightarrow$W sputtering ($Y_{O\rightarrow W}$=0.01 for the O$^+$ of $E_i = 90$ eV impact), and the sputtering yield for O$\rightarrow$Mo sputtering is $Y_{O\rightarrow Mo}$=0.04, which results in only 5% contribution of O to the total Mo erosion due to the He sputtering and negligible amount of sputtered W.

In the first experiment 8 samples (2 identical groups, 4 various surface roughness values in each of them) were irradiated for 40 minutes up to the fluence of F = 3.4x10^{24} m^{-2} in order to measure the Y$_{eff}$. Average values of plasma parameters during the exposure were $n_e \approx 3x10^{11}$cm^{-3}, $T_e \approx$ 5eV, $U_b \approx$ -100V. Samples with identical roughness values were placed at the opposite sides of the "circle" in order to take into account possible asymmetry of the plasma column. The mass loss measurements of the samples were conducted after the irradiation. The results are presented in the Fig.4. One can see that the measured sputtering yield is smaller for larger R$_a$ values. The lowest Y$_{eff}$ is observed for the highest roughness value 600 nm and is by a factor of 1.5 lower than for the smooth reference case (R$_a$ < 20nm). The dashed red line is the sputtering yield obtained using the Eckstein approximation formula for the SDTrimSP calculations [26]. One can see that even for the smooth case with R$_a$ < 20nm the measured sputtering yield is approximately 1.5 times lower than the SDTrimSP prediction. This has been already observed in previous PSI-2 experiments on W sputtering [6]. The most probable reason for this disagreement is the high uncertainty of the binary collisions approximation at these energies [32].

In the second experiment the penetration length of the sputtered Mo and its possible alterations during the exposure were measured for each type of roughness. For that 6 out of 8 graphite-Mo samples were replaced by W placeholders. Two Mo samples had the same roughness value and were positioned opposite to each other (see Fig.3c). The spectrometer was measuring the MoI at λ=386.4 nm light emission profiles along the facility axis. The spectrometer view was directed across the plasma column covering both Mo samples, therefore the emission intensity was doubled. The experiment was repeated 4 times for R_a = 110 nm, 280 nm, 600 nm and R_a < 20 nm. During the plasma irradiation ($\approx$40 min) both absolute light emission intensity and penetration depth ξ of Mo in the plasma stayed stable (ξ = 10.5 ±1.0 mm). Moreover, no visible changes were observed between various roughness cases. The minor variations observed in the absolute value of the light emission intensity were due to slow alterations of the plasma flux, since the ratio between the MoI line λ=386.4 nm and the HeI line λ=388.8 nm intensities stayed the same.

Moreover, the SEM analysis after all exposures has shown that the surface topography stayed the same during the irradiation for the case of R_a=600nm (see Fig.2b). This result is expected, since the layer of deposited Mo was only 100 nm and the plasma parameters have been chosen in a way to avoid its complete sputtering during the irradiation. Therefore, one could not expect seeing significant changes of the surface on the scale of 100 nm. At the same time, partial smoothing of the surface is visible for the case with the R_a = 110 nm (see Fig.2c). All SEM pictures were taken on two sides of the sample – the inner side of the circle and the outer one. The reason for this is the uneven distribution of plasma parameters over the sample. One can see in the Fig.3b that the U_{plasma} changes significantly in this region, which leads to the variations of the E_i by $\approx$5%. Furthermore, opposite sides of the sample experience different flux. One can notice black dots present on the inner side, which was subjected to a higher flux, even though the topography looks similar for the inner and outer sides of the sample. The conducted Rutherford backscattering (RBS) analysis confirmed that the Mo layer was eroded unevenly over the sample, however was not eroded completely (e.g. for the smooth case the lowest observed thickness of the Mo layer was $\approx$30 nm). Therefore, most likely the black dots observed are holes produced by the O desorption from the C substrate.

5. ERO2.0 simulation of the PSI-2 surface roughness experiments

In order to get the understanding of the interplay of processes contributing to the erosion of the samples, "machine-scale" ERO2.0 modelling has been conducted. The aim of this modelling was tracking of processes like sputtering of target materials (Mo, W) by plasma impurities (O) or re-deposition of W/Mo on the Mo rough surface. Moreover, due to the uneven distribution of plasma profiles over the sample it was important to estimate the distribution of the net erosion value over the sample surface. ERO2.0 confirmed the expected result: O sputtering contributes less than 5% to the total erosion of the Mo samples and the difference between the net and gross erosion values integrated over the sample is lower than 1%. The re-deposition of W on the samples surface is negligibly small according to the ERO2.0. This is also confirmed by the RBS measurements, which have shown <0.15 nm layer of W on all the samples. The distribution of the net erosion value over the sample surface is shown in Fig.5a. One can see that it is quite uneven over the sample surface with the maximum in the central part of it. This goes in line with visually observed changes of the sample surface and the RBS measurements (see Fig.5b,c) – the dark area resulting from higher incident fluence is visible on the sample and RBS measurements have shown that the Mo layer is thinner in the center of the sample than on the edges.

The "micro-scale" ERO2.0 runs have been conducted for the surface roughness types corresponding to those observed in the experiment. For this the results of AFM measurements (14x14 μm^2 using 6.5x10^4 cells or 70x70 μm^2 using 2.5x10^5 surface cells, therefore roughly ~2-3x10^4 Mo atoms in the surface cell) have been directly incorporated in ERO2.0 to define the rough surface (see Fig.6b). Processes like W and Mo re-deposition from the plasma have not been considered as they have been shown to be negligible by the machine-scale runs above and RBS measurements. As before, the sputtered particles have been traced until they leave the simulation volume or being re-deposited on the neighboring structures. 5x10^5 test particles have been tracked on every iteration step, each consisting of $\approx$1x10^9 "real" atoms. The side boundaries of the simulation box were periodic, the simulated area was much smaller than the characteristic size of plasma parameters gradient. The velocity vectors of the particles leaving the simulation volume through the upper boundary have been recorded as parameters of finally sputtered particles. The values of the Y_{eff} of the sputtered particles for considered roughness types are presented in Fig.6a. One can notice the maximum decrease of the effective sputtering yield by the factor of $\approx$1.3 for R_a=600 nm in comparison to the smooth reference. The effective angular distribution remains the same for various R_a values. This decrease of the Y_{eff} is smaller than the one measured in the experiment. The possible reason for this is the fact that AFM measurements are not able to catch fine details of the surface topography, especially for high R_a cases like R_a=600nm. This can be compared to the reduction of the D_{fract} of the surface structures, which in turn leads to the larger Y_{eff}, as was shown in the previous studies [21]. Time-resolved ERO2.0 simulations have shown that the surface topography in general stays stable over the exposure time with only the finest topography structures smoothed away, which is in line with the experimental observations.

6. Summary and conclusions

In the frame of this work the effect of surface roughness was implemented into the 3D Monte-Carlo PSI and plasma impurity transport code ERO2.0. Surface morphology is shown by ERO2.0 simulations to affect the effective sputtering yield Y_{eff} and angular distribution of sputtered particles: sharper (more "filigree") surface structures, both regular and irregular, lead to a suppression of the erosion. The surface modification algorithm was validated with ion-beam experiments on high-energy Ar$^+$ sputtering of cylindrical Si/Ta nanometer-scale structures under various incident angle cases. ERO2.0 simulation results have shown reasonable agreement with the corresponding SEM measurements.

Experiments at the linear plasma device PSI-2 have been conducted in order to test the influence of the surface morphology on the Y_{eff} and the effective angular distribution of sputtered particles. Validation of the ERO2.0 modelling with the PSI-2 experiments confirms the main trend: larger roughness of the sample surface leads to a reduced Y_{eff} (e.g. R_a=600 nm leads to decrease by ≈40% in comparison to the smooth case). In the case at hand, the Mo penetration depth variation with the sample roughness was found to be insignificant, which is due to relatively low aspect ratio of the surface structures. Surface topography evolution during the exposure was also negligible during the selected exposure time. Longer exposure of the deposited samples would unavoidably lead to the complete destruction of the Mo layer at some locations not conform with the idea of the experiment. Both observations are well in line with the conducted ERO2.0 modelling. Deeper insight into the problem can be obtained with further experiments and simulations using specifically-manufactured samples with bulk regular structures on the micrometer scale.

7. Acknowledgments

8. References

[1] Brezinsek, S., Journal of nuclear materials 463 (2015): 11-21.
[2] Mayer, M., et al. Journal of nuclear materials 363 (2007): 101-106.
[3] Hakola, A., et al. Physica Scripta 2014.T159 (2014): 014027.
[4] Kreter, A., et al. Plasma physics and controlled fusion 50.9 (2008): 095008.
[5] Schmid, K., M. Mayer, C. Adelhelm, et al., Nucl. Fusion 50 (2010) 105004.
[6] Eksaeva A., et al. Physica Scripta 2017 (T170), 014051
[7] Nishijima, D., et al. Journal of Nuclear Materials 415.1 (2011): S96-S99.
[8] Doerner, R. P., et al. Physica Scripta 2014.T159 (2014): 014040.
[9] Brooks, J. N., et all. No. CONF-900505--10. Argonne National Lab., 1990.
[10] Quan, S., et al. Contributions to Plasma Physics 57.8 (2017): 329-335.
[11] Cohen, R. H., et al. Contributions to Plasma Physics 40.3-4 (2000): 456-470.
[12] Arredondo Parra, R. "SIESTA: A new ion source setup and its application to erosion studies on first-wall materials for fusion reactors." (2019).
[13] Kirschner, A., et al. Nuclear Fusion 40.5 (2000): 989.
[14] Borodin, D., et al. Nuclear Materials and Energy 19 (2019): 510-515.
[15] Kirschner, A., et al. Nuclear Materials and Energy 18 (2019): 239-244.
[16] Borodin, D., et al. Physica Scripta 2007.T128 (2007): 127.
[17] Borodin, D., et al. Contributions to Plasma Physics 50.3-5 (2010): 432-438.
[18] Romazanov, J., et al. Nuclear Materials and Energy 18 (2019), 331–338.
[19] Romazanov, J., et al. Nuclear Materials and Energy 18 (2019): 331-338.
[20] Borodin, D., et al. Nuclear Materials and Energy 19 (2019): 510-515.
[21] Eksaeva A., et al. Nuclear Materials and Energy (2019) 19, 13-18
[22] Kreter, A., et al. Fusion science and technology 68.1 (2015): 8-14.
[23] Garcıa, R., et al. Surface science reports 47.6-8 (2002): 197-301.
[24] Betz, G., et al. International Journal of Mass Spectrometry and Ion Processes 140.1 (1994): 1-110.
[25] A. Goehlich, et al. Journal of Nuclear Materials, 266-269, (1999) 501-506
[26] W. Eckstein. Topics in Applied Physics, Vol. 110, (2007), 33-187
[27] Mutzke, A., et al. "SDTrimSP Version 6.00." (2019).
[28] Hayderer, G., et al. Review of scientific instruments 70.9 (1999): 3696-3700.
[29] Eksaeva A., et al. Nuclear Materials and Energy 12 (2017), 253-260
[30] E. Vassallo et al., Thin Solid Films 603 (2016) 173–179
[31] Goldstein, J.I., et al. Scanning electron microscopy and X-ray microanalysis. Springer, 2017.
[32] Doerner, R. P., et al. Journal of Nuclear Materials 438 (2013): S272-S275.
[33] D. Borodin, R. Doerner, D. Nishijima, et al., J. Nucl. Mater. 415, S219 (2011).
[34] Dai, Shuyu, et al. Journal of Nuclear Materials 463 (2015): 372-376.
[35] D. Dellasega, et al, , J. Appl. Phys. 112 (2012) 084328. doi:10.1063/1.4761842.
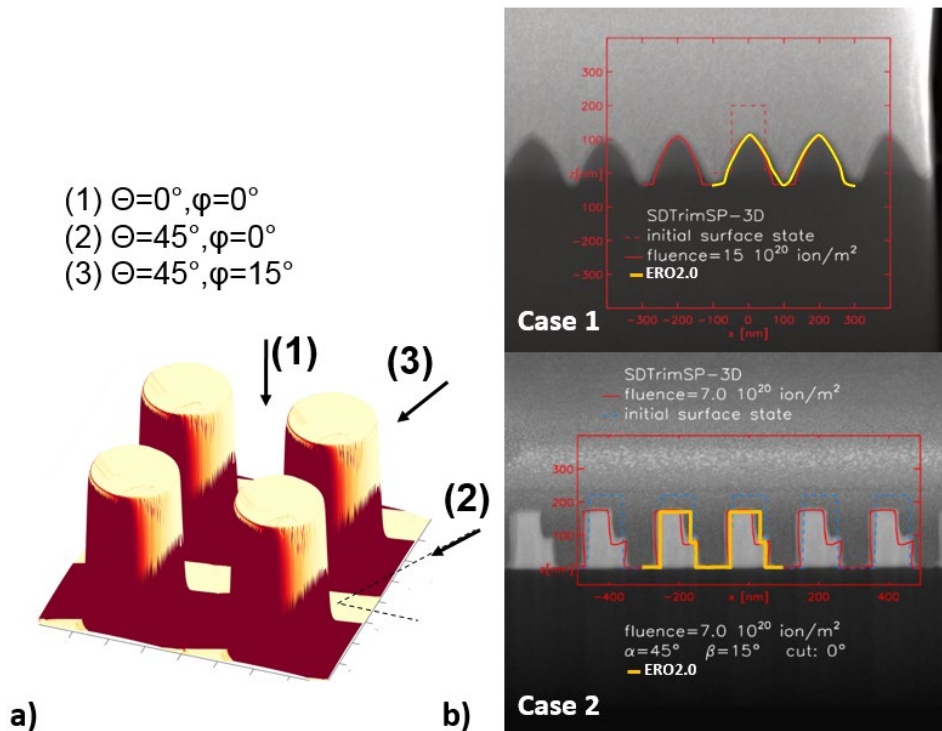
Fig. 1. a) Shadowing pattern calculated in ERO2.0 for the case (3) of inclined Ar ion beam incidence. The three incidence angle cases are marked as (1), (2), (3). b) ERO2.0 simulation results for 2 cases from the ion beam experiments [13], along with a comparison to SDTrimSP-3D and experimental SEM measurement. Case 1: Ar->Si 5 keV, normal incidence (fluence = 15×10^{20} m^{-2}); Case 2: Ar->Ta 5 keV, $\Theta=45°$ $\varphi=15°$ (fluence = 7×10^{20} m^{-2}).
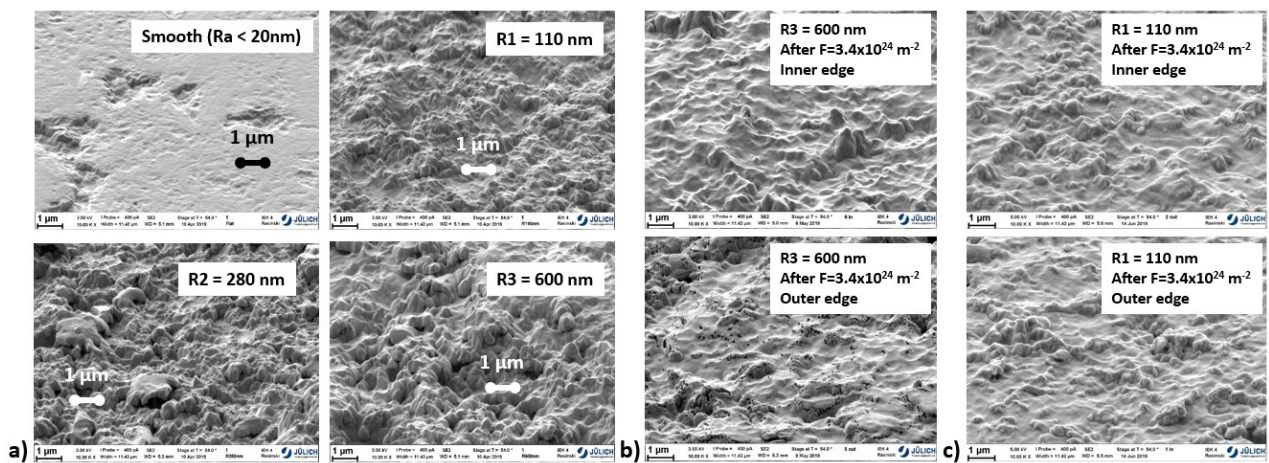
Fig. 2. SEM measurements results for the rough surfaces a) before the exposure, all roughness cases; b) roughness case R_3 – R_a = 600 nm after the He plasma exposure of the fluence F = 3.4×10^{24} m^{-2}, "outer" edge of the sample and "inner" edge of the sample (see Fig. 4). c) roughness case R_1 – R_a = 110 nm after the He plasma exposure of the fluence F = 3.4×10^{24} m^{-2}, "outer" edge of the sample and "inner" edge of the sample.
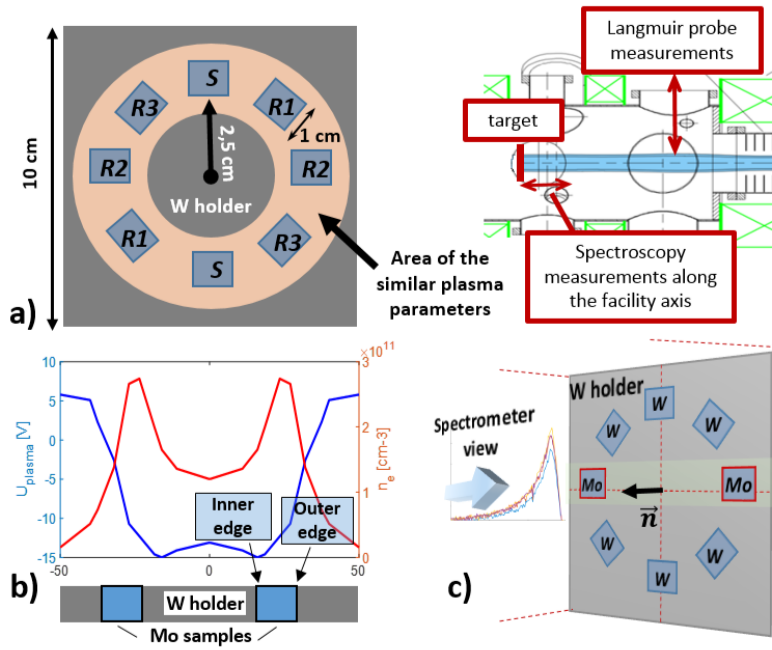
Fig. 3. a) Left: target configuration - the W sample holder with samples of various roughness types (S – smooth, $R_a < 20$ nm, $R_1 – R_a = 110$ nm, $R_2 – R_a = 280$ nm, $R_3 – R_a = 600$ nm). Right – part of the PSI-2 scheme near the target with spectroscopy measurement area marked. b) PSI-2 plasma density and plasma potential profiles with the samples marked. c) Target configuration for the 2nd experiment with two Mo samples of the same R_a (experiment was conducted for each R_a value).
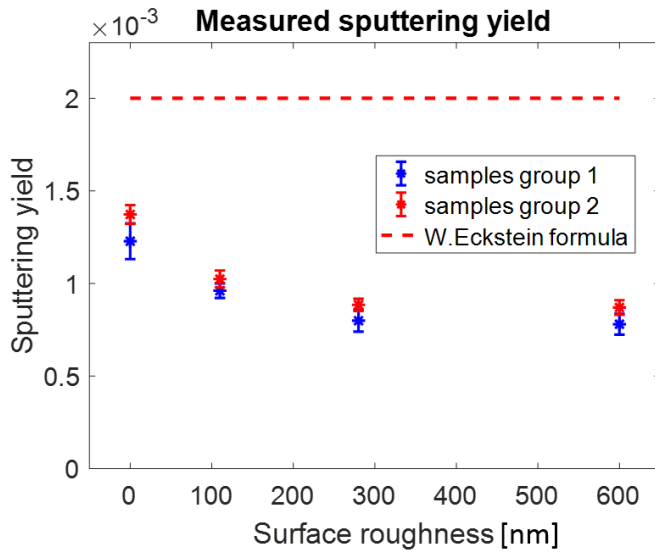

Fig. 4. Effective sputtering yield Y_{eff} measured in the PSI-2 experiments for the surface roughness R_a =110 nm, 280 nm, 600 nm and a smooth reference with $R_a<20$nm (He→Mo irradiation, $E_{in}≈90$ eV). The red dashed line is the W.Eckstein [24] sputtering yield value.
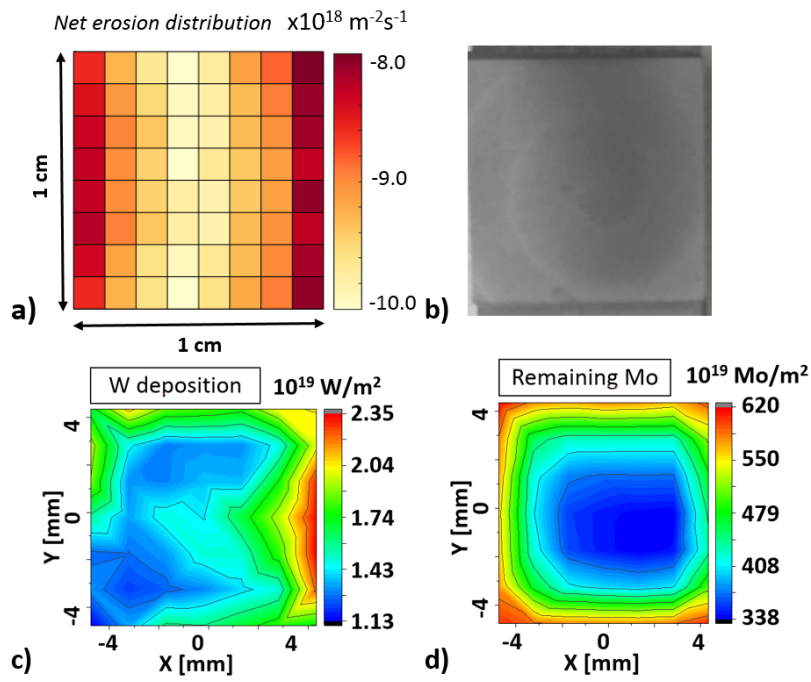
Figure 5. a) Distribution of the Mo net erosion over the sample surface simulated by ERO2.0. b) Photo of the sample surface with R_a=600nm after the fluence=3.4x10^{24}m^{-2}; c) RBS measurements of the W layer thickness of the sample with $R_a < 20$ nm; d) RBS measurements of the Mo layer thickness of the sample with $R_a < 20$ nm]
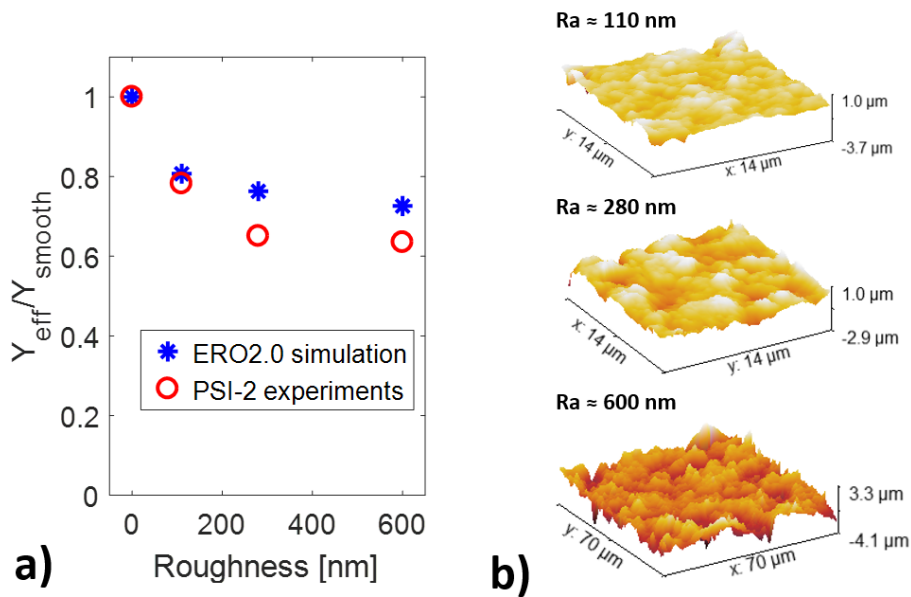

Fig. 6. a) Ratio of the Y_{eff} from the rough surface to the Y_{smooth} for R_a =110 nm, 280 nm, 600 nm. ERO2.0 simulation results and the measured values from the PSI-2 experiments. b) Surface topography for R_a =110 nm, 280 nm, 600 nm obtained with the AFM measurements.